Hindawi
Journal of Nanomaterials
Volume 2022, Article ID 4903486, 12 pages
https://doi.org/10.1155/2022/4903486

Research Article

Heat Transfer Analysis of the MHD Stagnation Point Flow of a Non-Newtonian Tangent Hyperbolic Hybrid Nanofluid past a Non-Isothermal Flat Plate with Thermal Radiation Effect

Abdullah Dawar,[1] **Saeed Islam**,[1] **Ahmed Alshehri**,[2] **Ebenezer Bonyah**,[3] **and Zahir Shah**[4]

[1]*Department of Mathematics, Abdul Wali Khan University, Mardan, 23200 Khyber Pakhtunkhwa, Pakistan*
[2]*Department of Mathematics, Faculty of Sciences, King Abdulaziz University, Jeddah 21589, Saudi Arabia*
[3]*Department of Mathematics Education, University of Education Winnebakumasi-(Kumasicompus), Kumasi 00233, Ghana*
[4]*Department of Mathematical Sciences, University of Lakki Marwat, Lakki Marwat, 28420 Khyber Pakhtunkhwa, Pakistan*

Correspondence should be addressed to Ebenezer Bonyah; ebbonya@gmail.com

Received 21 December 2021; Accepted 9 May 2022; Published 25 May 2022

Academic Editor: Domenico Acierno

Heat transfer phenomena are used in a variety of industries, including chemical devices, shipbuilding, power plants, electronic devices, and medicinal plants. Propylene glycol, engine oil, water, and ethylene glycol are common single-phase heat transfer liquids used in a variety of industries, including chemical process industries and thermal power plants. Therefore, the authors are interested in investigating the magnetohydrodynamic flow of a water-based hybrid nanofluid containing ferrous and graphene oxide nanoparticles past a flat plate. The stagnation points, as well as the effects of magnetic field and thermal radiation are taken into account in this analysis. The non-Newtonian tangent hyperbolic flow, which is laminar and incompressible, is also considered to investigate the non-Newtonian behavior of the hybrid nanofluid flow. The proposed model has been solved analytically with the help of HAM. The convergence of HAM is shown with the help of figure. The hydrothermal characteristics of hybrid nanofluid flow past a nonisothermal flat plate at a stagnation point are affected by the necessary parameters. The results show that the boosting volume fractions of the ferrous and graphene oxide nanoparticles have significantly reduced the velocity field, while the thermal field has increased with the augmenting volume fractions of the ferrous and graphene oxide nanoparticles. The increasing power-law index has augmented the viscosity of the non-Newtonian hybrid nanofluid flow due to which the velocity field escalated. However, this impact is opposite for the thermal field. Due to the direct relation between the Weissenberg number and relaxation time, the greater Weissenberg number has reduced the velocity profile, while increased the thermal field.

1. Introduction

Because of various applications in healthcare and engineering, such as microelectronics, solar collectors, process industries, cancer therapy, heat exchangers, and power production, the mechanisms of heat exchange incorporating nanomaterials have piqued the interest of researchers. Regular liquids such as glycol mixtures, engine oil, and water had moderately poor thermal properties and inadequate capacity to attain higher thermal efficiency. The use of nanoparticles to develop the thermal conductivity of various cooling fluids is a contemporary method. Nowadays, temperature distribution plays an essential function in a variety of scientific and technical disciplines. Heat transfer phenomena have a wide range of applications in sectors, shipbuilding, electronic devices, power plants, medicinal, and chemical devices. To design heat exchangers and discover the optimal geometry, radiators, condensers, evaporators, and boilers, heat transfer analysis and the related cooling process become invaluable. Propylene glycol, engine oil, water, and ethylene glycol are common single-phase heat transfer liquids used in a variety of chemical process industries and thermal power plants. Due to its low thermal conductivity, the single-phase traditional liquids are acknowledged to have poor heat transmission ability. This improvement in working fluid heat transport is critical for achieving energy and cost reductions. In order to boost-up the thermal conductivity of the base fluids, many researchers have worked to resolve these issues and improve the thermal conductivity of the base fluids. Solid materials have higher thermal conductivity than those of liquids. As a result, dispersing microscopic solid particles into a base liquid is a novel technique to increase the thermal conductivity of the base fluids. Khan et al. [1] investigated the Casson nanofluid flow past a rotating disk. Shah et al. [2] addressed the applications of radius, heat flux, and mass flux of the water-based copper nanoparticles. Gul T et al. [3] investigated the flow of carbon nanotube nanofluid past a rotating cone and disk. Sowmya et al. [4] addressed the effects of convective condition and internal heat generation in a nanofluid flow past a porous fin. Ashraf et al. [5] analyzed the magnetohydrodynamic peristaltic flow of the blood-based magnetite nanoparticles. Dawar et al. [6] studied the unsteady flow of carbon nanotube nanofluid with the magnetic field impact. Rasool and Wakif [7] examined the electromagnetohydrodynamic second-grade nanofluid flow over a Riga plate. Alghamdi et al. [8] presented the magnetohydrodynamic flow of sodium alginate-based nanofluid bounded by slender surface with heat source impact. Rout et al. [9] analyzed the water- and kerosene-based nanofluid flow with viscous dissipation. Alshomrani and Gul [10] investigated the dissipative flow of water-based Al_2O_3 and Cu nanoparticles past a stretching cylinder with convective condition. Further related analyses can be studied in [11–14].

Hybrid nanofluid is a class of nanofluids, developed by integrating a certain class of nanoparticles inside a functional fluid which has recently been used. Two different nanomaterials are suspended in a conventional fluid to create hybrid nanofluids. Hybrid nanofluids are widely used in a diversity of disciplines of engineering as well as refrigeration, space planes, biomedicals, machining coolant, motor cooling, heat pipe reduction in medicine, and high-performance boats. Jana et al. [15] investigated the conductive nanomaterials like copper and gold nanoparticles and their hybrids. Khashi'ie et al. [16] analyzed heat transfer of a magnetohydrodynamic flow of a water-based hybrid nanofluid comprehending Cu and Al_2O_3 nanoparticles. Their results show that the suction factor has a significant impact of heat transfer analysis. Additionally, they have computed the stability analysis as well. Nawaz and Nazir [17] studied the magnetohydrodynamic flow of an ethylene-based hybrid nanofluid flow containing MoS_2 and SiO_2 nanoparticles. They compared MoS_2/ethylene-based and MoS_2-SiO_2/ethylene-based hybrid nanofluids. Their results showed that the thermal performance is greater for the MoS_2-SiO_2/ethylene-based as compared to MoS_2/ethylene-based. Manjunatha et al. [18] presented the comparative analysis of the magnetohydrodynamic flows of Cu-H_2O nanofluid and Cu-Al_2O_3/H_2O hybrid nanofluid. They found that the nanoparticle volume fraction of the nanofluid and hybrid nanofluid has enhanced the velocity and thermal fields. Usman et al. [19] proposed the comparative analysis of the magnetohydrodynamic flow of a Cu/H_2O nanofluid, Al_2O_3/H_2O nanofluid, and Cu-Al_2O_3/H_2O hybrid nanofluid. They claimed that the velocity fields of Cu-Al_2O_3/H_2O have dominant role on other nanofluids; however, this impact is reverse for thermal profile. Iqbal et al. [20] offered the comparative analysis of magnetohydrodynamic flows of SiO_2/H_2O nanofluid and MoS_2-SiO_2/H_2O hybrid nanofluid considering different shapes of the nanoparticles. Their results showed that the nanofluid has slower flow as compared to hybrid nanofluid. Additionally, the lower temperature is observed for brick-shaped nanoparticles of the nanofluid, while the blade-shaped nanoparticle of the hybrid nanofluid has extreme temperature. Ghadikolaei et al. [21] offered the comparative investigation of magnetohydrodynamic flow of Cu/H_2O and hybrid nanofluid containing TiO_2-Cu/H_2O at a stagnation point. They also considered three different shapes of the nanoparticles named as platelets, bricks, and cylinders. It is clear from of this research that using platelet-shaped nanoparticles is more effective. Gul et al. [22] addressed the magnetohydrodynamic flow of hybrid nanofluid containing Cu and Fe_3O_4. Their results showed that the nanoparticle volume fractions of Cu and Fe_3O_4 have significantly improved the thermal transmission and velocity field. Alghamdi et al. [23] addressed the comparative analysis of the magnetohydrodynamic flows of blood-based Cu nanofluid and blood-based Cu-CuO hybrid nanofluid. It has been introduced that the hybrid nanofluid flow has more effective thermal conductivity in a contracting channels. Acharya [24] probed the application of solar energy toward a hybrid nanofluid flow containing alumina and copper nanoparticles. In another article, Acharya and Mabood [25] addressed the water-based hybrid nanofluid flow containing ferrous and graphene oxide nanoparticles. Thumma et al. [26] investigated the Cu-CuO nanoparticles past a porous extending surface. Acharya et al. [27, 28] analyzed the nanofluid and hybrid nanofluid flows under the impact of magnetic field.

According to the authors' knowledge, there is no study based on magnetohydrodynamic flow of water-based hybrid nanofluid containing ferrous and graphene oxide nanoparticles past a flat plate. The stagnation point along with the impacts of magnetic field and thermal radiation is taken in this consideration. The non-Newtonian tangent hyperbolic flow which is laminar and incompressible is also considered to investigate the non-Newtonian behavior of the hybrid nanofluid flow. The present analysis is composed of mathematical modeling which is shown in Section 2. HAM solution and convergence of HAM are presented in Sections 3 and 4, respectively. Section 5 is composed of results and discussion. In the last, the concluding remarks are shown in Section 6.

2. Model Formulation

Consider the stagnation point flow of a water-based hybrid nanofluid containing graphene oxide (GO) and ferrous

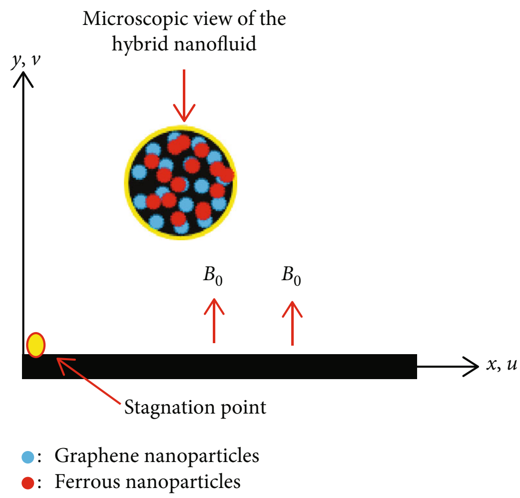

FIGURE 1: Geometry of the hybrid nanofluid flow.

(Fe_3O_4) nanoparticles past a flat plate. The flat plate is chosen to be a nonisothermal. The non-Newtonian tangent hyperbolic model is taken to be laminar and incompressible. u and v are the velocity components which are considered along x- and y-directions, respectively. A magnetic field $B = (0, B_0, 0)$ is considered normal to the flow direction. The ambient velocity of the fluid flow along x-direction is $u_e(x) = cx$, where c is the positive constant. The wall temperature $T_w(x) = T_\infty + bx$ varies linearly along x-direction in which b is the positive constant and T_∞ is the ambient temperature. Furthermore, the Hall current and thermal radiation effects are also considered. Following the above assumption, the leading equations are stated. Figure 1 shows the geometry of the hybrid nanofluid flow.

$$\frac{\partial u}{\partial x} + \frac{\partial v}{\partial y} = 0,$$

$$u\frac{\partial u}{\partial x} + v\frac{\partial u}{\partial y} = u_e\frac{du_e}{dx} + \frac{\mu_{hnf}}{\rho_{hnf}}\left[(1-n)\frac{\partial^2 u}{\partial y^2} + \sqrt{2}n\Gamma\frac{\partial u}{\partial y}\frac{\partial^2 u}{\partial y^2}\right] - \frac{\sigma_{hnf}B_0^2}{\rho_{hnf}}(u-u_e),$$

$$u\frac{\partial T}{\partial x} + v\frac{\partial T}{\partial y} = \alpha_{nf}\frac{\partial^2 T}{\partial y^2} - \frac{1}{(\rho C_p)_{hnf}}\frac{\partial q_r}{\partial y} + \frac{\sigma_{hnf}B_0^2}{(\rho C_p)_{hnf}}u^2 + \frac{\mu_{hnf}}{(\rho C_p)_{hnf}}\left[(1-n)\left(\frac{\partial u}{\partial y}\right)^2 + \frac{n\Gamma}{\sqrt{2}}\left(\frac{\partial u}{\partial y}\right)^3\right]. \quad (1)$$

The relevance boundary conditions are defined as

$$\left\{\begin{array}{c} u = 0, v = 0, T = T_w \, at \, y = 0, \\ u \longrightarrow u_e, T \longrightarrow T_\infty \, as \, y \longrightarrow \infty. \end{array}\right\} \quad (2)$$

TABLE 1: The numerical values of the thermophysical properties of base fluids and nanoparticles [29].

Base fluids/ nanoparticles	ρ (kg.m^{-3})	C_p (J.kg^{-1}.K^{-1})	k [W.m^{-1}.K^{-1}]	σ ((Ω m)$^{-1}$)
H_2O	997	4180	0.6071	0.005
Fe_3O_4	5180	670	9.7	25000
GO	2250	2100	2500	1×107

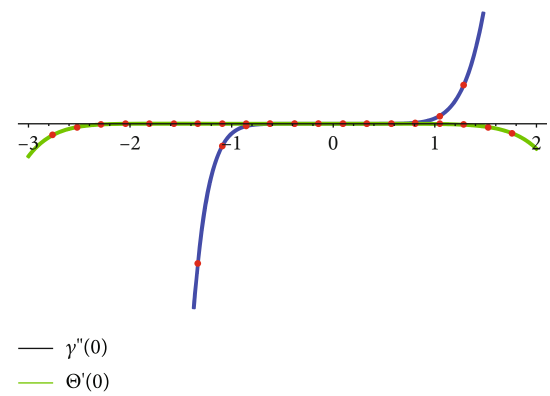

FIGURE 2: $h-$ curves for velocity and temperature profiles.

The radiative heat flux q_r is defined as

$$q_r = -\frac{4\sigma^*}{3k^*}\frac{\partial T^4}{\partial y}. \quad (3)$$

By using the Taylor series expansion, T^4 can be written as

$$T^4 \approx 4T_\infty^3 T - 3T_\infty^4. \quad (4)$$

For the simulation of hybrid nanofluid flow, the thermophysical properties are defined as

$$\left\{\begin{array}{c} \frac{\mu_{hnf}}{\mu_f} = \frac{1}{(1-\phi_1-\phi_2)^{2.5}}, \frac{\rho_{hnf}}{\rho_f} = (1-\phi_1-\phi_2) + \frac{\rho_{p1}\phi_1 + \rho_{p2}\phi_2}{\rho_f}, \\ \frac{(\rho C_p)_{hnf}}{(\rho C_{\widehat{p}})_f} = (1-\phi_1-\phi_2) + \frac{(\rho C_{\widehat{p}})_{p1}\phi_1 + (\rho C_p)_{p2}\phi_2}{(\rho C_{\widehat{p}})_f}, \\ \frac{k_{hnf}}{k_f} = \frac{(k_{p1}\phi_1 + k_{p2}\phi_2/\phi_1+\phi_2) + 2k_f + 2(k_{p1}\phi_1 + k_{p2}\phi_2) - 2(\phi_1+\phi_2)k_f}{(k_{p1}\phi_1 + k_{p2}\phi_2/\phi_1+\phi_2) + 2k_f - (k_{p1}\phi_1 + k_{p2}\phi_2) + (\phi_1+\phi_2)k_f}, \\ \frac{\sigma_{hnf}}{\sigma_f} = 1 + \frac{3((\sigma_{p1}\phi_1 + \sigma_{p2}\phi_2/\sigma_f) - (\phi_1+\phi_2))}{2 + (\sigma_{p1}\phi_1 + \sigma_{p2}\phi_2/(\phi_1+\phi_2)\sigma_f) - (\sigma_{p1}\phi_1 + \sigma_{p2}\phi_2/\sigma_f) + (\phi_1+\phi_2)}, \end{array}\right\} \quad (5)$$

where $p1$ and $p2$ represent Fe_3O_4 and GO nanoparticles, respectively, and ϕ_1 and ϕ_2 are the nanoparticle volume fractions of Fe_3O_4 and GO, respectively. The numerical values of the thermophysical properties are defined in Table 1.

Table 2: Impacts of ϕ_1, ϕ_2, We, n, and M on $\sqrt{\mathrm{Re}_x} C_{fx}$.

ϕ_1	ϕ_2	We	n	M	$\sqrt{\mathrm{Re}_x} C_{fx}$
0.01					1.10639
0.02					1.10443
0.03					1.10381
	0.01				1.05003
	0.02				1.06374
	0.03				1.07768
		0.2			0.92856
		0.3			0.95661
		0.4			0.98308
			0.2		1.09048
			0.3		0.99856
			0.4		0.89890
				0.2	1.11986
				0.3	1.14266
				0.4	1.17459

The similarity transformations are defined as

$$
\begin{aligned}
u &= cx\Upsilon'(\zeta), \\
u &= -\sqrt{c\nu_f}\,\Upsilon(\zeta), \\
\Theta(\zeta) &= \frac{T - T_\infty}{T_w - T_\infty}, \\
\zeta &= y\sqrt{\frac{c}{\nu_f}}.
\end{aligned}
\tag{6}
$$

Using the above similarity transformations, the leading equations are transformed as

$$
\begin{aligned}
&\frac{1}{(1-\phi_1-\phi_2)^{2.5}}\left[(1-n)+nWe\Upsilon''\right]\Upsilon''' \\
&\quad + \left[(1-\phi_1-\phi_2)+\frac{\rho_{p1}\phi_1+\rho_{p2}\phi_2}{\rho_f}\right]\left(\Upsilon\Upsilon''+1-\Upsilon'^2\right) - M^2 \\
&\quad \cdot \left[1+\frac{3\left(\left(\sigma_{p1}\phi_1+\sigma_{p2}\phi_2/\sigma_f\right)-(\phi_1+\phi_2)\right)}{2+\left(\sigma_{p1}\phi_1+\sigma_{p2}\phi_2/(\phi_1+\phi_2)\sigma_f\right)-\left(\sigma_{p1}\phi_1+\sigma_{p2}\phi_2/\sigma_f\right)+(\phi_1+\phi_2)}\right] \\
&\quad \cdot \left(\Upsilon'-1\right) = 0, \\
&\left[\frac{\left(k_{p1}\phi_1 +_{p2}\phi_2/\phi_1+\phi_2\right)+2k_f+2\left(k_{p1}\phi_1+k_{p2}\phi_2\right)-2(\phi_1+\phi_2)k_f}{\left(k_{p1}\phi_1+k_{p2}\phi_2/\phi_1+\phi_2\right)+2k_f-\left(k_{p1}\phi_1+k_{p2}\phi_2\right)+(\phi_1+\phi_2)k_f}+\frac{4}{3}Rd\right]\Theta'' \\
&\quad + \Pr\left[(1-\phi_1-\phi_2)+\frac{\left(\rho C_{\widehat{p}}\right)_{p1}\phi_1+\left(\rho C_p\right)_{p2}\phi_2}{\left(\rho C_{\widehat{p}}\right)_f}\right]\left(\Upsilon\Theta'-\Upsilon'\Theta\right) \\
&\quad + \frac{Ec\Pr}{(1-\phi_1-\phi_2)^{2.5}}\begin{pmatrix}(1-n)\Upsilon''^2 \\ +\dfrac{n}{2}\mathrm{We}\,\Upsilon''^3\end{pmatrix} + \Pr M^2 Ec \\
&\quad \cdot \left[1+\frac{3\left(\left(\sigma_{p1}\phi_1+\sigma_{p2}\phi_2/\sigma_f\right)-(\phi_1+\phi_2)\right)}{2+\left(\sigma_{p1}\phi_1+\sigma_{p2}\phi_2/(\phi_1+\phi_2)\sigma_f\right)-\left(\sigma_{p1}\phi_1+\sigma_{p2}\phi_2/\sigma_f\right)+(\phi_1+\phi_2)}\right]\Upsilon'^2 \\
&= 0,
\end{aligned}
\tag{7}
$$

Table 3: Impacts of ϕ_1, ϕ_2, We, n, Ec, Rd, and M on $(1/\sqrt{\mathrm{Re}_x})Nu_x$.

ϕ_1	ϕ_2	We	n	M	Ec	Rd	$(1/\sqrt{\mathrm{Re}_x})Nu_x$
0.01							0.42728
0.02							0.40796
0.03							0.38505
	0.01						0.42748
	0.02						0.40809
	0.03						0.38515
		0.2					0.60811
		0.3					0.60089
		0.4					0.59368
			0.2				0.32874
			0.3				0.37203
			0.4				0.41532
				0.2			0.32291
				0.3			0.31672
				0.4			0.30806
					0.2		-0.34687
					0.3		-0.77920
					0.4		-1.21753
						0.2	0.24689
						0.3	0.17259
						0.4	0.08544

with boundary conditions

$$
\left\{\begin{matrix} \Upsilon(0)=0,\ \Upsilon'(0)=0,\ \Upsilon'(\infty)=1, \\ \Theta(0)=1, \Theta(\infty)=0. \end{matrix}\right\}
\tag{8}
$$

The dimensionless parameters are defined as

$$
\begin{aligned}
Rd &= \frac{4\sigma^* T_\infty^3}{k^* k_f}, \\
\Pr &= \frac{\nu_f}{\alpha_f}, \\
M &= \sqrt{\frac{\sigma_f B_0^2}{\rho_f c}}, \\
\mathrm{We} &= \sqrt{2}c\Gamma\, \mathrm{Re}_x^{1/2}, \\
\mathrm{Re}_x &= \frac{x u_e(x)}{\nu_f}, \\
Ec &= \frac{u_e^2}{\left(C_p\right)_f (T_w - T_\infty)}.
\end{aligned}
\tag{9}
$$

Physical quantities of importance like skin friction C_{fx} and Nusselt number Nu_x are defined as

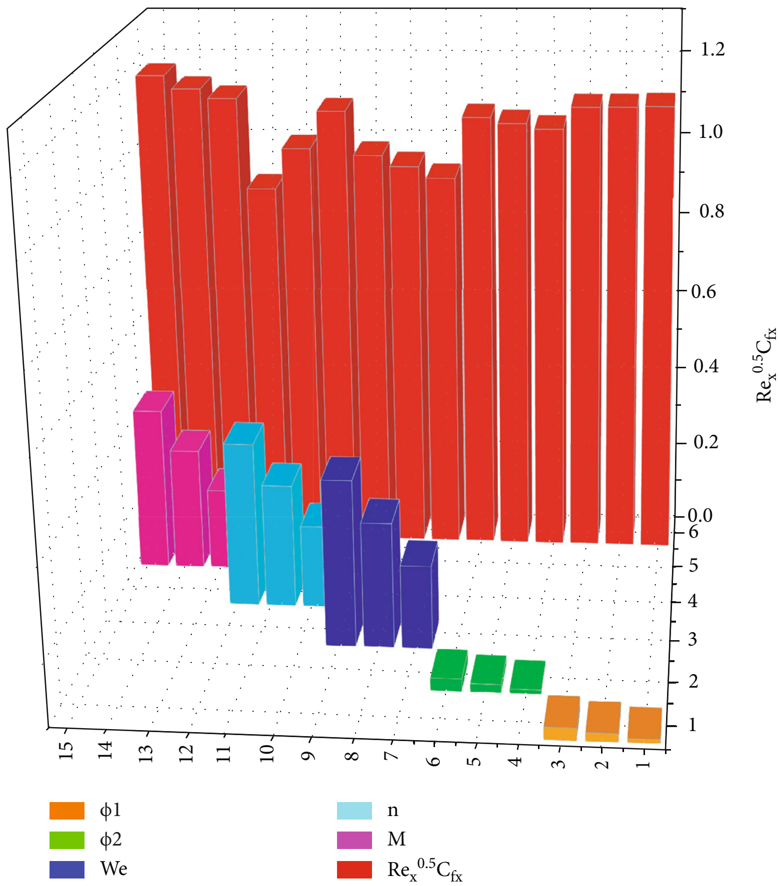

FIGURE 3: Impacts of ϕ_1, ϕ_2, We, n, and M on $\sqrt{\mathrm{Re}_x}C_{fx}$.

$$C_{fx} = \frac{\mu_{hnf}}{\rho_{hnf}u_e^2}\left[(1-n)\frac{\partial u}{\partial y} + \frac{n\Gamma}{\sqrt{2}}\left(\frac{\partial u}{\partial y}\right)^2\right]\Bigg|_{y=0},$$
$$Nu_x = -\frac{x}{(T_w - T_\infty)}\left[\frac{k_{hnf}}{k_f}\frac{\partial T}{\partial y} + \frac{4\sigma^*}{3k^* k_f}\frac{\partial T^4}{\partial y}\right]\Bigg|_{y=0}. \tag{10}$$

Using the similarity transformations defined in equation (6), the above quantities are reduced to

$$\mathrm{Re}_x^{1/2}C_{fx} = \frac{1}{(1-\phi_1-\phi_2)^{2.5}\left((1-\phi_1-\phi_2) + \left(\rho_{p1}\phi_1 + \rho_{p2}\phi_2/\rho_f\right)\right)} \cdot \left[(1-n)\Upsilon''(0) + \frac{nWe}{2}\Upsilon''^2(0)\right],$$

$$\mathrm{Re}_x^{-1/2}Nu_x = -\left[\frac{(k_{p1}\phi_1 +_{p2}\phi_2/\phi_1+\phi_2) + 2k_f + 2(k_{p1}\phi_1 + k_{p2}\phi_2) - 2(\phi_1+\phi_2)k_f}{(k_{p1}\phi_1 + k_{p2}\phi_2/\phi_1+\phi_2) + 2k_f - 2(k_{p1}\phi_1 + k_{p2}\phi_2) + (\phi_1+\phi_2)k_f} + \frac{4}{3}Rd\right]\Theta'(0). \tag{11}$$

3. HAM Solution

To attain the analytical solution of the proposed model along with the relevant boundary conditions, HAM method which was introduced by Liao [30] is applied. The initial guesses and linear operators are defined as

$$\Upsilon_0(\zeta) = -1 + \zeta + e^{-\zeta},$$
$$\Theta_0(\zeta) = e^{-\zeta},$$
$$L_\Upsilon = \Upsilon''' - \Upsilon',$$
$$L_\Theta = \Theta'' - \Theta, \tag{12}$$

satisfying

$$L_\Upsilon\left[\widehat{\mathfrak{R}}_1 + \widehat{\mathfrak{R}}_2 e^{-\zeta} + \widehat{\mathfrak{R}}_3 e^{\zeta}\right] = 0,$$
$$L_\Theta\left[\widehat{\mathfrak{R}}_4 e^{-\zeta} + \widehat{\mathfrak{R}}_5 e^{\zeta}\right] = 0, \tag{13}$$

where $\widehat{\mathfrak{R}}_1 - \widehat{\mathfrak{R}}_5$ are constants.

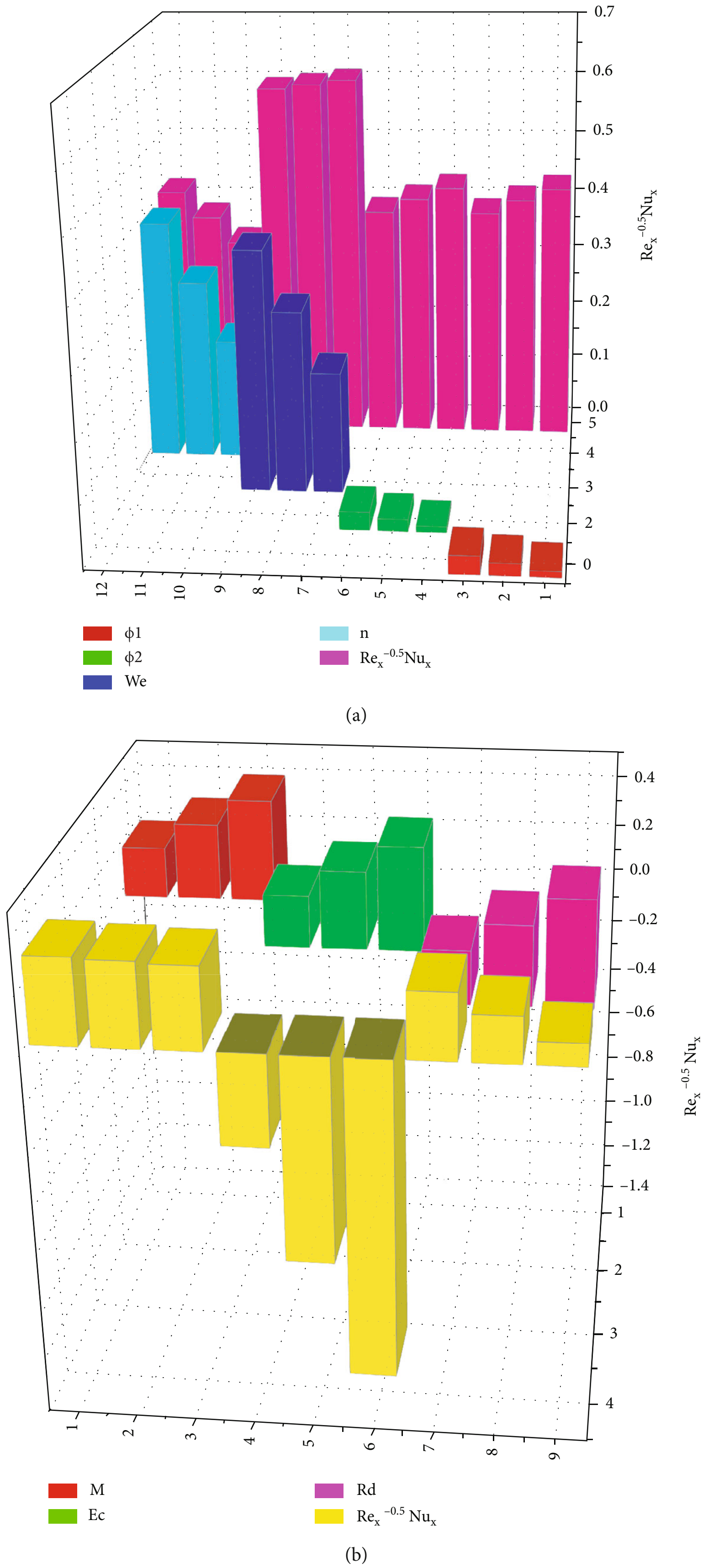

Figure 4: (a) Impacts of ϕ_1, ϕ_2, We, and n on $(1/\sqrt{\mathrm{Re}_x})Nu_x$. (b) Impacts of Ec, Rd, and M on $(1/\sqrt{\mathrm{Re}_x})Nu_x$.

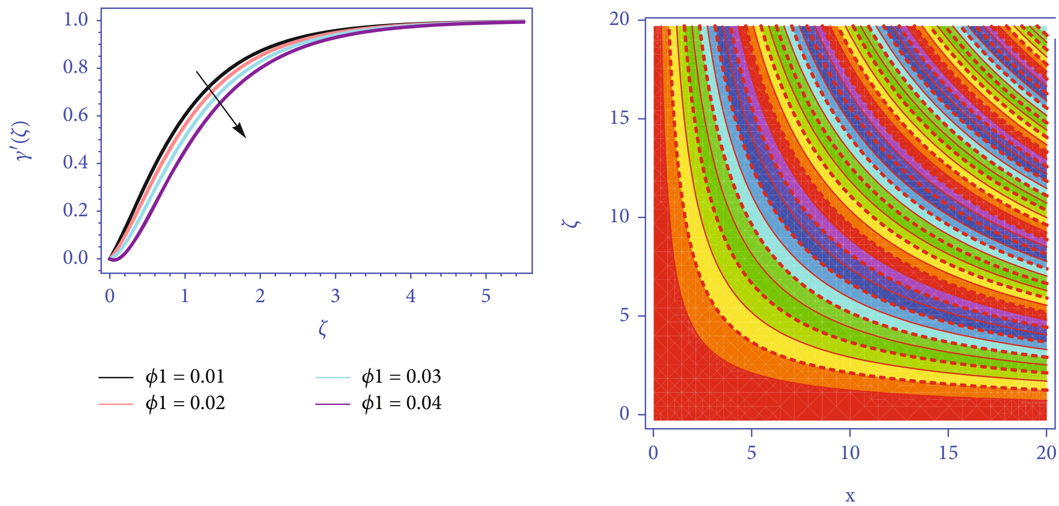

(a) (b)

Figure 5: (a) Effect of ϕ_1 on $\Upsilon'(\zeta)$. (b) Streamline patterns for ϕ_1.

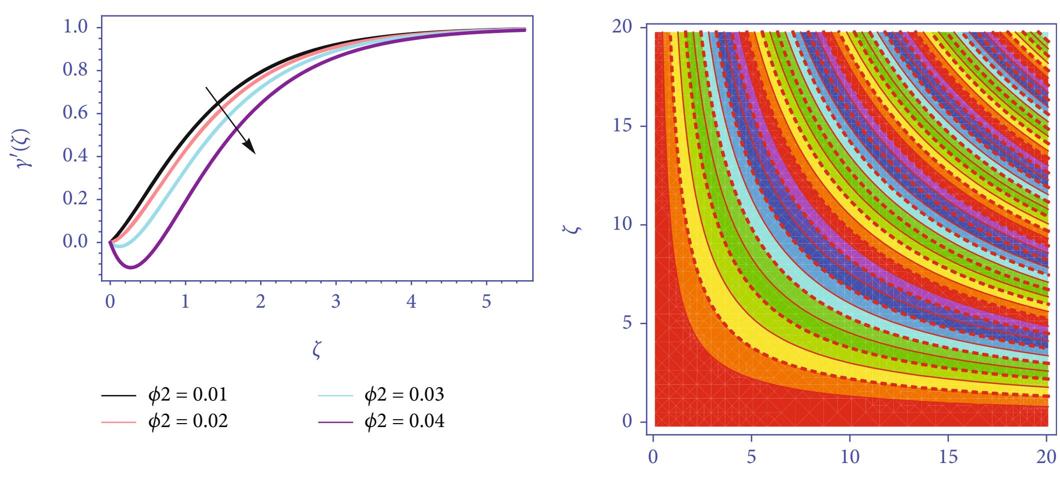

(a) (b)

Figure 6: (a) Effect of ϕ_2 on $\Upsilon'(\zeta)$. (b) Streamline patterns for ϕ_2.

4. HAM Convergence

Homotopy analysis method guarantees the convergence analysis of the highly linear and nonlinear differential equations. The auxiliary parameter h insures the convergence area of the modeled problem. The convergence areas for velocity and temperature profiles are $-1.0 \leq h_{\Upsilon} \leq 1.0$ and $-2.5 \leq h_{\Theta} \leq 1.5$, respectively, as shown in Figure 2.

5. Results and Discussion

This part explains how the hydrothermal characteristics of hybrid nanofluid flow past a nonisothermal flat plate at a stagnation point are affected by the necessary parameters. To demonstrate physically accurate effects, thermal radiation and magnetic field are added. The hybrid nanofluid flow contains ferrous (Fe_3O_4) and graphene oxide (GO) nanoparticles and water (H_2O) is used as base fluid. In the present analysis, the default values are considered as $M = 1.0$, $n = 0.5$, $\mathrm{We} = 0.6$, $\mathrm{Pr} = 6.2$, $\phi_1 = \phi_2 = 0.05$, $Ec = 0.3$, and $Rd = 0.7$.

The effects of the significant parameters on $\sqrt{\mathrm{Re}_x}C_{fx}$ and $Nu_x/\sqrt{\mathrm{Re}_x}$ are shown in Tables 2 and 3. The augmenting volume fraction of the Fe_3O_4 nanoparticles declines the surface drag force, while the augmenting volume fraction of the GO nanoparticles boosts up the skin friction coefficient. The augmenting impacts of Fe_3O_4 and GO nanoparticle volume fractions are found against heat transfer rate. The greater Weissenberg number We augments $\sqrt{\mathrm{Re}_x}C_{fx}$; however, $Nu_x/\sqrt{\mathrm{Re}_x}$ reduces with the higher We. A similar impact of n is found for $\sqrt{\mathrm{Re}_x}C_{fx}$ and $Nu_x/\sqrt{\mathrm{Re}_x}$. The greater

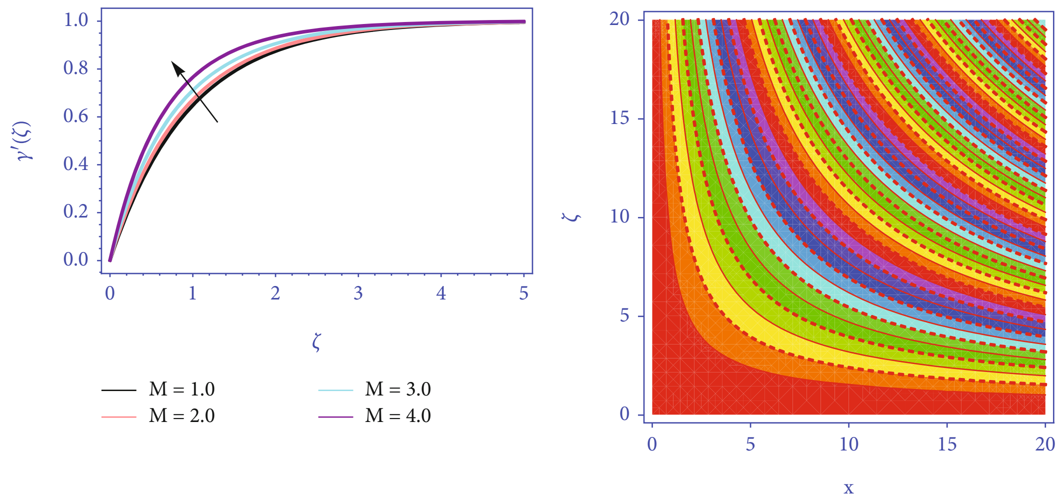

(a) (b)

Figure 7: (a) Effect of M on $\Upsilon'(\zeta)$. (b) Streamline patterns for M.

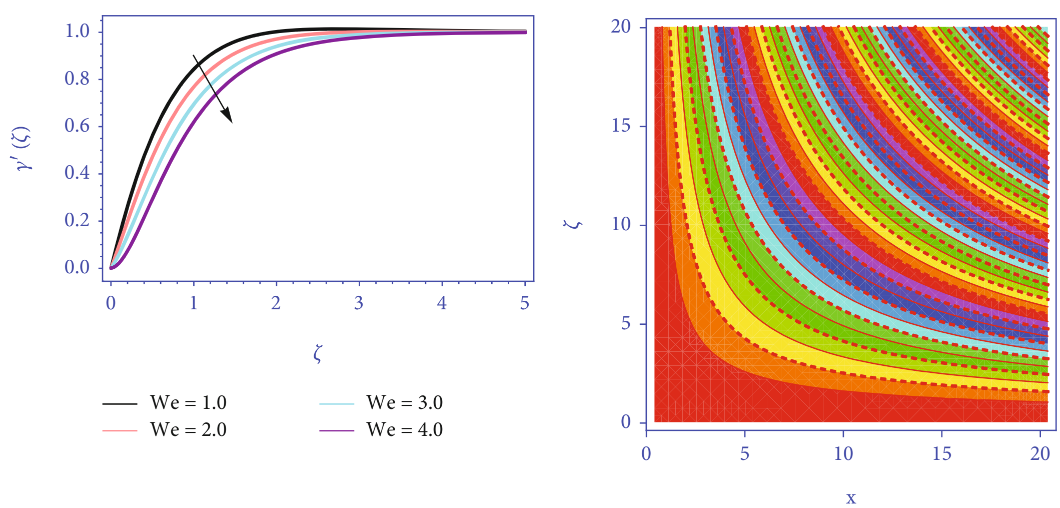

(a) (b)

Figure 8: (a) Effect of We on $\Upsilon'(\zeta)$. (b) Streamline patterns for We.

magnetic parameter M augments $\sqrt{\mathrm{Re}_x}C_{fx}$, while an opposite trend is observed for $Nu_x/\sqrt{\mathrm{Re}_x}$. Also, the greater Eckert number Ec and thermal radiation parameter Rd have declining impacts on $Nu_x/\sqrt{\mathrm{Re}_x}$. Figures 3 and 4 are displayed in order to clarify the variation in $\sqrt{\mathrm{Re}_x}C_{fx}$ and $Nu_x/\sqrt{\mathrm{Re}_x}$ via different embedded parameters. Figure 5(a) shows the impact of ϕ_1 on $\Upsilon'(\zeta)$ when $\phi_2 = 0.05$. The augmenting ϕ_1 declines $\Upsilon'(\zeta)$. The increasing ϕ_1 declines the boundary layer thickness, which consequently reduces $\Upsilon'(\zeta)$. Figure 5(b) shows the streamline patterns for ϕ_1 when $\phi_2 = 0.05$. Figure 6(a) shows the impact of ϕ_2 on $\Upsilon'(\zeta)$ when $\phi_1 = 0.05$. A similar impact as of Fe_3O_4 nanoparticle is found here. Figure 6(b) shows the streamline patterns for ϕ_2 when $\phi_1 = 0.05$. Figure 7(a) signifies the consequence of M on $\Upsilon'(\zeta)$. The escalating magnetic parameter boosts up the velocity field. As the dynamic growth upsurges, the boundary layer of the velocity profile gets thinner, showing that the magnetic parameter augments the flow mobility near the heated plate. The present model is computed along with stagnation point flow, thus the augmenting impact of the magnetic parameter has been reported here. Figure 7(b) shows the streamline patterns for M when $\phi_1 = \phi_2 = 0.05$. Figure 8(a) signposts the effect of We on $\Upsilon'(\zeta)$. The augmenting We reduces $\Upsilon'(\zeta)$. The maximum value of the parameter We increases $\Upsilon'(\zeta)$, because We is directly related to the relaxation time Γ. The relaxation time of the examined non-Newtonian hybrid nanofluid has increased. As a result of this physical property, the water-based flow encounters extra barrier in developing easily across the flow boundary, lowering the hybrid nanofluid velocity. Figure 8(b) shows the streamline patterns for We when

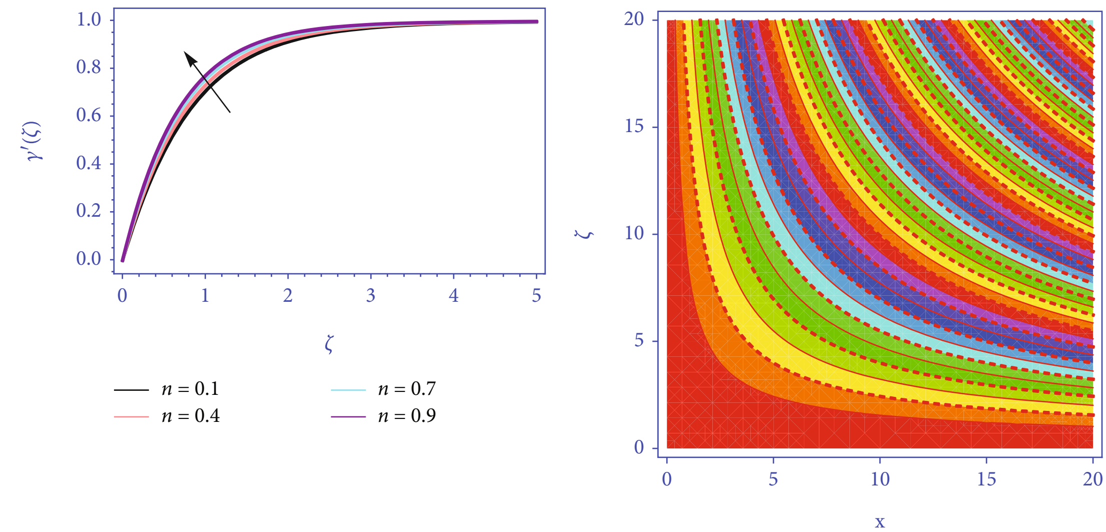

(a) (b)

Figure 9: (a) Effect of n on $\Upsilon'(\zeta)$. (b) Streamline patterns for n.

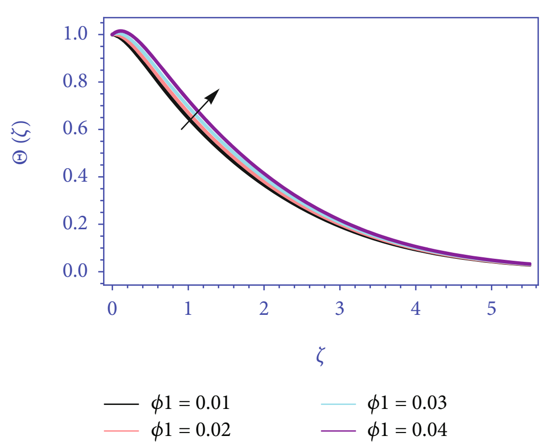

Figure 10: Effect of ϕ_1 on $\Theta(\zeta)$.

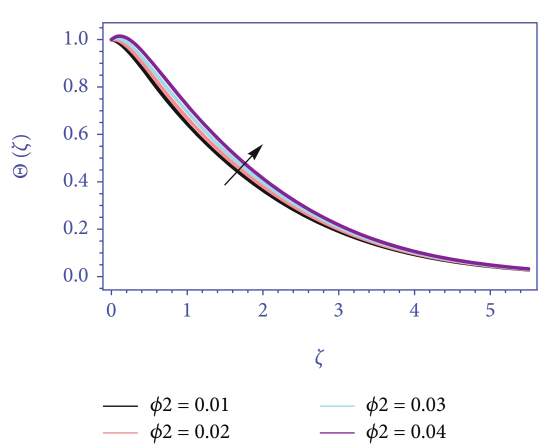

Figure 11: Effect of ϕ_2 on $\Theta(\zeta)$.

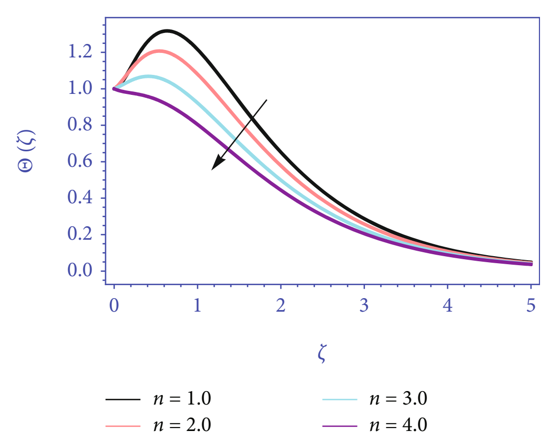

Figure 12: Effect of n on $\Theta(\zeta)$.

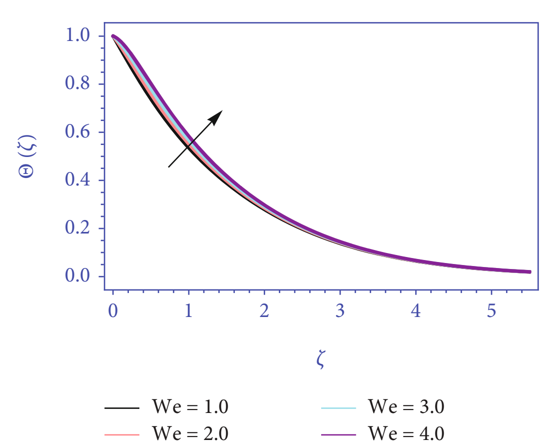

Figure 13: Effect of We on $\Theta(\zeta)$.

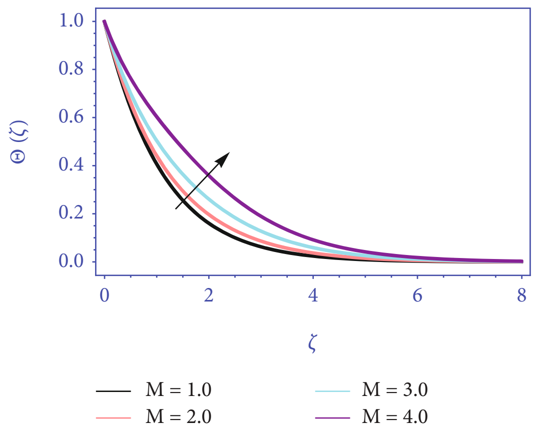

Figure 14: Effect of M on $\Theta(\zeta)$.

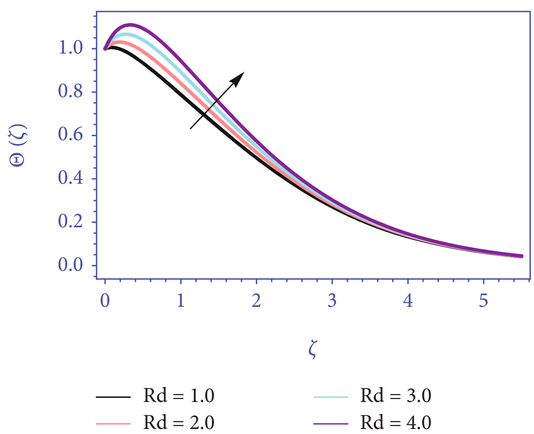

Figure 15: Effect of Rd on $\Theta(\zeta)$.

$\phi_1 = \phi_2 = 0.05$. Figure 9(a) displays the effect of n on $\Upsilon'(\zeta)$. The escalating n shows augmenting conduct against $\Upsilon'(\zeta)$. The numerical value of the power-law index parameter is specified for two different fluids, namely, pseudoplastic $(n < 1)$ and dilatant $(n > 1)$. Physically, the escalating n interconnects an important augmentation in the viscosity of the non-Newtonian hybrid nanofluid flow. That is why the velocity boundary layer thickness is declined; as a result, $\Upsilon'(\zeta)$ is augmented. Figure 9(b) shows the streamline patterns for n when $\phi_1 = \phi_2 = 0.05$. Figure 10 shows the effect of ϕ_1 on $\Theta(\zeta)$ when $\phi_2 = 0.05$. The increasing ϕ_1 augments $\Theta(\zeta)$. Figure 11 shows the effect of volume fraction ϕ_2 on $\Theta(\zeta)$ when $\phi_1 = 0.05$. The increasing ϕ_2 augments $\Theta(\zeta)$. Figure 12 shows the effect of power-law index n on $\Theta(\zeta)$ when $\phi_1 = \phi_2 = 0.05$. The rising n declines $\Theta(\zeta)$. The increasing n thickens the temperature boundary layer which diminishes the temperature of the hybrid nanofluid flow. Thus, a declining impact is found here. Figure 13 exhibits the effect of We on $\Theta(\zeta)$ when $\phi_1 = \phi_2 = 0.05$. The increasing We augments $\Theta(\zeta)$. The increasing We shows that the increased quantity of thermal energy provided to the nanofluidic system due to resistive nanofluid motion can explain this thermal behavior physically. Figure 14 displays the impact of M on $\Theta(\zeta)$ when $\phi_1 = \phi_2 = 0.05$. The augmenting M escalates

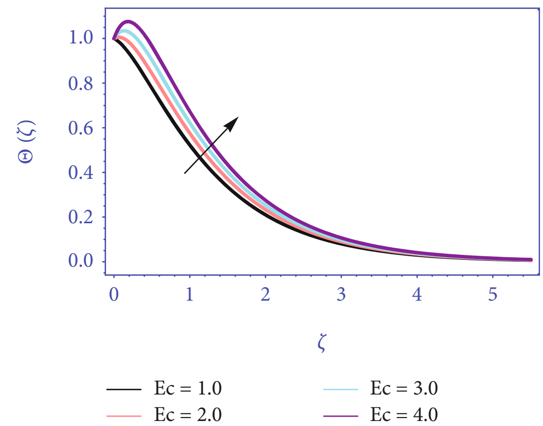

Figure 16: Effect of Ec on $\Theta(\zeta)$.

$\Theta(\zeta)$ of the hybrid nanofluid flow. Physically, as the magnetic parameter increases, the movement of particles of hybrid nanofluid escalates. Thus, both the thermal boundary and temperature of the hybrid nanofluid augment. Figure 15 designates the effect of Rd on $\Theta(\zeta)$ when $\phi_1 = \phi_2 = 0.05$. The increasing radiation parameter boosts up $\Theta(\zeta)$. Physically, the increasing radiation parameter augments the surface heat of the hybrid nanofluid flow which makes the hybrid nanofluid hotter. Thus, the escalating conduct is observed here. Figure 16 displays the effect of Eckert number Ec on $\Theta(\zeta)$ when $\phi_1 = \phi_2 = 0.05$. The increasing Eckert number augments $\Theta(\zeta)$. The link between kinetic energy and enthalpy in a flow is described by the Eckert number. It denotes the effort expended in converting kinetic energy to internal energy in the face of viscous fluid forces. An increase in the Eckert number implies that the fluid has a high kinetic energy; consequently, the intermolecular collisions take place which enhances the particles vibration. So, the increased molecule collisions increase heat dissipation in the boundary layer region, causing $\Theta(\zeta)$ to climb.

6. Conclusion

The magnetohydrodynamic flow of water-based hybrid nanofluid containing ferrous and graphene oxide nanoparticles past a flat plate has been studied in this article. The stagnation point along with the impacts of magnetic field and thermal radiation is taken in this consideration. The non-Newtonian tangent hyperbolic flow which is laminar and incompressible is also considered to investigate the non-Newtonian behavior of the hybrid nanofluid flow. The hydrothermal characteristics of the hybrid nanofluid flow past a nonisothermal flat plate at a stagnation point are affected by the necessary parameters. Key points of this analysis are as follows:

(1) The increasing volume fractions of the ferrous and graphene oxide nanoparticles have significantly reduced the velocity field, while the thermal field has increased with the augmenting volume fractions of the ferrous and graphene oxide nanoparticles

(2) The augmenting magnetic parameter has considerably enhanced the velocity and thermal fields

(3) Due to the direct relation between the Weissenberg number and relaxation time, the greater Weissenberg number has reduced the velocity profile, while increased the thermal field

(4) The increasing power-law index has augmented the viscosity of the non-Newtonian hybrid nanofluid flow due to which the velocity field escalated. However, this impact is opposite for the thermal field

(5) The augmenting Eckert number and thermal radiation parameter have increased the thermal field

Nomenclature

Constants:	b, c
Magnetic field strength:	B_0 (kg s^{-2} A^{-1})
Skin friction coefficient:	C_{fx}
Specific heat:	C_p (J kg^{-1} K^{-1})
Eckert number:	Ec
Mean absorption coefficient:	k^*
Thermal conductivity:	k (Wm^{-1}K^{-1})
Magnetic parameter:	M
Power-law index:	n
Nusselt number:	Nu_x
Prandtl number:	Pr
Radiative heat flux:	q_r (Wm^{-2})
Radiation parameter:	Rd
Local Reynolds number:	Re
Temperature:	T (K)
Free-stream velocity:	$u_e(x)$ (ms^{-1})
Velocity components:	(u, v) (ms^{-1})
Weissenberg number:	We
Cartesian coordinates:	(x, y) (m).

Greek Symbols

Kinetic viscosity:	ν (m^{2}s^{-1})
Dimensionless temperature:	θ
Nanoparticle volume fraction:	ϕ
Dynamic viscosity:	μ (kgm^{-1}s^{-1})
Time-dependent material:	Γ (s)
Density:	ρ (kgm^{-3})
Stefan–Boltzmann constant:	σ^*
Electrical conductivity:	σ (Sm^{-1})
Similarity variable:	ζ.

Subscripts

Base fluid:	f
Nanoparticles:	$p1, p2$
Wall boundary condition:	w
Free-stream condition:	∞.

Data Availability

All the supporting data are within the manuscript.

Conflicts of Interest

The authors declare that they have no conflict of interest.

References

[1] U. Khan, S. Bilal, A. Zaib, O. D. Makinde, and A. Wakif, "Numerical simulation of a nonlinear coupled differential system describing a convective flow of Casson gold–blood nanofluid through a stretched rotating rigid disk in the presence of Lorentz forces and nonlinear thermal radiation," *Numerical Methods for Partial Differential Equations*, vol. 38, no. 3, pp. 308–328, 2020.

[2] N. A. Shah, I. L. Animasaun, J. D. Chung, A. Wakif, F. I. Alao, and C. S. K. Raju, "Significance of nanoparticle's radius, heat flux due to concentration gradient, and mass flux due to temperature gradient: the case of Water conveying copper nanoparticles," *Scientific Reports*, vol. 11, no. 1, pp. 1–11, 2021.

[3] T. Gul, R. S. Gul, W. Noman et al., "CNTs-nanofluid flow in a rotating system between the gap of a disk and cone," *Physica Scripta*, vol. 95, no. 12, article 125202, 2020.

[4] G. Sowmya, B. J. Gireesha, S. Sindhu, and B. C. Prasannakumara, "Investigation of Ti6Al4V and AA7075 alloy embedded nanofluid flow over longitudinal porous fin in the presence of internal heat generation and convective condition," *Communications in Theoretical Physics*, vol. 72, no. 2, article 025004, 2020.

[5] M. U. Ashraf, M. Qasim, A. Wakif, M. I. Afridi, and I. L. Animasaun, "A generalized differential quadrature algorithm for simulating magnetohydrodynamic peristaltic flow of blood-based nanofluid containing magnetite nanoparticles: a physiological application," *Numerical Methods for Partial Differential Equations*, 2020.

[6] A. Dawar, Z. Shah, W. Khan, M. Idrees, and S. Islam, "Unsteady squeezing flow of magnetohydrodynamic carbon nanotube nanofluid in rotating channels with entropy generation and viscous dissipation," *Advances in Mechanical Engineering*, vol. 11, no. 1, Article ID 168781401882310, 2019.

[7] G. Rasool and A. Wakif, "Numerical spectral examination of EMHD mixed convective flow of second-grade nanofluid towards a vertical Riga plate using an advanced version of the revised Buongiorno's nanofluid model," *Journal of Thermal Analysis and Calorimetry*, vol. 143, no. 3, pp. 2379–2393, 2021.

[8] M. Alghamdi, A. Wakif, T. Thumma, U. Khan, D. Baleanu, and G. Rasool, "Significance of variability in magnetic field strength and heat source on the radiative-convective motion of sodium alginate-based nanofluid within a Darcy-Brinkman porous structure bounded vertically by an irregular slender surface," *Case Studies in Thermal Engineering*, vol. 28, article 101428, 2021.

[9] B. C. Rout, S. R. Mishra, and T. Thumma, "Effect of viscous dissipation on Cu-water and Cu-kerosene nanofluids of axisymmetric radiative squeezing flow," *Heat Transfer—Asian Research*, vol. 48, no. 7, pp. 3039–3054, 2019.

[10] A. S. Alshomrani and T. Gul, "A convective study of Al2O3-H2O and Cu- H2O nano-liquid films sprayed over a stretching cylinder with viscous dissipation," *The European Physical Journal Plus*, vol. 132, no. 11, pp. 1–16, 2017.

[11] M. Bilal, A. Saeed, T. Gul, I. Ali, W. Kumam, and P. Kumam, "Numerical approximation of microorganisms hybrid nanofluid flow induced by a wavy fluctuating spinning disc," *Coatings*, vol. 11, p. 1032, 2021.

[12] M. Jawad, A. Saeed, M. Bilal, T. Gul, A. Khan, and S. Nasir, “The impact of magnetohydrodynamic on bioconvection nanofluid flow with viscous dissipation and joule heating effects,” *Engineering Research Express*, vol. 3, no. 1, article 015030, 2021.

[13] T. Gul, J. U. Rahman, M. Bilal et al., “Viscous dissipated hybrid nanoliquid flow with Darcy–Forchheimer and forced convection over a moving thin needle,” *AIP Advances*, vol. 10, article 105308, 2020.

[14] M. Bilal, T. Gul, A. Alsubie, and I. Ali, “Axisymmetric hybrid nanofluid flow with heat and mass transfer amongst the two gyrating plates,” *ZAMM-Journal of Applied Mathematics and Mechanics/Zeitschrift für Angewandte Mathematik und Mechanik*, vol. 101, no. 11, article e202000146, 2021.

[15] S. Jana, A. Salehi-Khojin, and W. H. Zhong, “Enhancement of fluid thermal conductivity by the addition of single and hybrid nano-additives,” *Thermochimica Acta*, vol. 462, no. 1-2, pp. 45–55, 2007.

[16] N. S. Khashi'ie, N. M. Arifin, R. Nazar, E. H. Hafidzuddin, N. Wahi, and I. Pop, “Magnetohydrodynamics (MHD) axisymmetric flow and heat transfer of a hybrid nanofluid past a radially permeable stretching/shrinking sheet with Joule heating,” *Chinese Journal de Physique*, vol. 64, pp. 251–263, 2020.

[17] M. Nawaz and U. Nazir, “An enhancement in thermal performance of partially ionized fluid due to hybrid nano-structures exposed to magnetic field,” *AIP Advances*, vol. 9, no. 8, article 085024, 2019.

[18] S. Manjunatha, B. Ammani Kuttan, S. Jayanthi, A. Chamkha, and B. J. Gireesha, “Heat transfer enhancement in the boundary layer flow of hybrid nanofluids due to variable viscosity and natural convection,” *Heliyon*, vol. 5, no. 4, article e01469, 2019.

[19] M. Usman, M. Hamid, T. Zubair, R. Ul Haq, and W. Wang, “Cu-Al2O3/water hybrid nanofluid through a permeable surface in the presence of nonlinear radiation and variable thermal conductivity via LSM,” *International Journal of Heat and Mass Transfer*, vol. 126, pp. 1347–1356, 2018.

[20] Z. Iqbal, E. N. Maraj, E. Azhar, and Z. Mehmood, “A novel development of hybrid (MoS2–SiO2/H2O) nanofluidic curvilinear transport and consequences for effectiveness of shape factors,” *Journal of the Taiwan Institute of Chemical Engineers*, vol. 81, pp. 150–158, 2017.

[21] S. S. Ghadikolaei, M. Yassari, H. Sadeghi, K. Hosseinzadeh, and D. D. Ganji, “Investigation on thermophysical properties of Tio2–Cu/H2O hybrid nanofluid transport dependent on shape factor in MHD stagnation point flow,” *Powder Technology*, vol. 322, pp. 428–438, 2017.

[22] T. Gul, M. Kashifullah, W. Bilal, M. I. Alghamdi, T. A. Asjad, and T. Abdeljawad, “Hybrid nanofluid flow within the conical gap between the cone and the surface of a rotating disk,” *Scientific Reports*, vol. 11, no. 1, p. 1180, 2021.

[23] W. Alghamdi, A. Alsubie, P. Kumam, A. Saeed, and T. Gul, “MHD hybrid nanofluid flow comprising the medication through a blood artery,” *Scientific Reports*, vol. 11, no. 1, pp. 1–13, 2021.

[24] N. Acharya, “On the flow patterns and thermal behaviour of hybrid nanofluid flow inside a microchannel in presence of radiative solar energy,” *Journal of Thermal Analysis and Calorimetry*, vol. 141, no. 4, pp. 1425–1442, 2020.

[25] N. Acharya and F. Mabood, “On the hydrothermal features of radiative Fe3O4–graphene hybrid nanofluid flow over a slippery bended surface with heat source/sink,” *Journal of Thermal Analysis and Calorimetry*, vol. 143, no. 2, pp. 1273–1289, 2021.

[26] T. Thumma, S. R. Mishra, and O. A. Bég, “ADM solution for Cu/CuO–water viscoplastic nanofluid transient slip flow from a porous stretching sheet with entropy generation, convective wall temperature and radiative effects,” *Journal of Applied and Computational Mechanics*, pp. 1–15, 2021.

[27] N. Acharya, K. Das, and P. K. Kundu, “Framing the effects of solar radiation on magneto-hydrodynamics bioconvection nanofluid flow in presence of gyrotactic microorganisms,” *Journal of Molecular Liquids*, vol. 222, pp. 28–37, 2016.

[28] N. Acharya, R. Bag, and P. K. Kundu, “On the impact of nonlinear thermal radiation on magnetized hybrid condensed nanofluid flow over a permeable texture,” *Applied Nanoscience*, vol. 10, no. 5, pp. 1679–1691, 2020.

[29] N. Acharya, “Spectral quasi linearization simulation on the hydrothermal behavior of hybrid nanofluid spraying on an inclined spinning disk,” *Partial Differential Equations in Applied Mathematics*, vol. 4, article 100094, 2021.

[30] S. Liao, “An optimal homotopy-analysis approach for strongly nonlinear differential equations,” *Communications in Nonlinear Science and Numerical Simulation*, vol. 15, no. 8, pp. 2003–2016, 2010.